Research Article

Zhong Xu*, Zhenpu Huang, Changjiang Liu*, Xiaowei Deng*, David Hui*, Yuting Deng, Min Zhao, and Libing Qin

Experimental study on mechanical properties and microstructures of steel fiber-reinforced fly ash-metakaolin geopolymer-recycled concrete

https://doi.org/10.1515/rams-2021-0050
received June 17, 2021; accepted July 01, 2021

Abstract: Geopolymer cementitious materials and recycled aggregate are typical representatives of material innovation research in the engineering field. In this study, we experimentally investigated a method to improve the performance of geopolymer-recycled aggregate concrete (GRAC). The recycled concrete aggregates and steel fiber (SF), fly ash (FA), metakaolin (MK), and sodium silicate solution were used as the main raw materials to prepare fiber-reinforced geopolymer-recycled aggregate concrete (FRGRAC). First, the orthogonal test was carried out to study the GRAC, and the optimal mix proportion was found. Second, building on the optimal mix proportion, the effects of the SF content on the slump, 7 and 28 days compressive strength, tensile strength, and flexural strength of FRGRAC were further studied. Finally, the microscopic mechanism of FRGRAC was studied by scanning electron microscopy (SEM). The study results indicate that the slump continues to decrease as the fiber content increases, but the compressive strength, tensile strength, and flexural strength increase to a certain extent. Through SEM analysis, it is found that SF restrains the development of cracks and improves the strength of concrete.

Keywords: SF, geopolymer, recycled concrete, orthogonal test, microstructure

1 Introduction

With the growth of the global population and the acceleration of urbanization, the development of the construction industry has been greatly promoted, but this has also exacerbated the problem of environmental pollution. Statistics shows that the annual output of global cement production will increase to 6.1 billion tons in 2050, which means extremely high CO_2 emissions (7% of global carbon emissions) [1,2]. On the other hand, urbanization needs to demolish old buildings, which will undoubtedly generate a lot of construction waste. The stacking of construction waste will consume a lot of land resources, and if not handled properly, it will cause harm to soil and water [3,4].

The emergence of GRAC can be one of the promising solutions for the above problems. Geopolymers are mainly derived from industrial production wastes. Combining these raw materials rich in silicon and aluminum compounds, such as FA, MK, etc., with an alkali solution will cause polymerization. After polymerization, geopolymer concrete (GPC) can be formed with a higher strength than that of ordinary Portland concrete (OPC) [5]. Therefore, replacing cement with a geopolymer can be an ideal choice, which can greatly reduce the emission of CO_2 [6]. On the other hand, recycled aggregate concrete (RAC) can also solve the problem of construction waste disposal. The

* **Corresponding author: Zhong Xu,** College of Environment and Civil Engineering, Chengdu University of Technology, Chengdu 610059, China, e-mail: xuzhong@cdut.edu.cn
* **Corresponding author: Changjiang Liu,** School of Civil Engineering, Guangzhou University, Guangzhou 510006, China, e-mail: cjliu@gzhu.edu.cn
* **Corresponding author: Xiaowei Deng,** Department of Civil Engineering, The University of Hong Kong, Pokfulam, Hong Kong 999077, China, e-mail: xwdeng@hku.hk
* **Corresponding author: David Hui,** Department of Mechanical Engineering, University of New Orleans, New Orleans, LA 70148, United States of America, e-mail: dhui@uno.edu
Zhenpu Huang: College of Environment and Civil Engineering, Chengdu University of Technology, Chengdu 610059, China, e-mail: 1720304378@qq.com
Yuting Deng: College of Environment and Civil Engineering, Chengdu University of Technology, Chengdu 610059, China, e-mail: 852699341@qq.com
Min Zhao: College of Environment and Civil Engineering, Chengdu University of Technology, Chengdu 610059, China, e-mail: 12898554@qq.com
Libing Qin: Engineering Technology Research Center, Sichuan Mingyang Construction Engineering Management Co. Ltd., Chengdu 610059, China, e-mail: qlb20054115@126.com

test blocks of waste concrete are usually crushed, cleaned, graded, and mixed according to a certain proportion to prepare recycled concrete aggregate (RCA). The concrete made by RCA is called RAC [7,8]. A combination of GPC and RAC can greatly solve the pollution problem in civil engineering construction.

However, due to the high porosity of the residual mortar in RCA, the strength of RCA is generally low, which affects the strength of GRAC [9,10]. GRAC also exhibits brittleness similar to OPC [11,12]. These limit the application of GRAC. The addition of fiber can reduce the brittleness of concrete and effectively improve the strength of concrete. At present, the study on using fiber to improve GPC [13–18] and RAC [19–22] has matured. But, most of the current research in the field of GRAC focuses on improving its strength, crack resistance [23–27], etc., and the use of fiber to improve GRAC is still lacking.

This article presents using steel fiber (SF) and FA–MK matrix geopolymer cementing material to prepare fiber-reinforced geopolymer recycled aggregate concrete (FRGRAC). Based on the orthogonal test considering three factors and three levels and considering the 7 days compressive strength as the index, the influence factors of GRAC compressive strength are studied and the optimal mix proportion is found. Based on this, the effects of the SF content on the slump of FRGRAC, compressive strength, tensile strength, and flexural strength of 28 days were investigated. Furthermore, its microscopic mechanism was analyzed by SEM. It is expected that the results from this study can help establish a foundation for the FRGRAC application in engineering practice in the future.

2 Materials and methodology

2.1 Experimental materials

Class II FA was provided by Chuanxing Mineral Powder Factory. MK calcined at 900°C was produced by Henan Jinao Refractory Co., Ltd. Concentrated sodium silicate solution with a modulus of 2.2 was 40%, and the purity

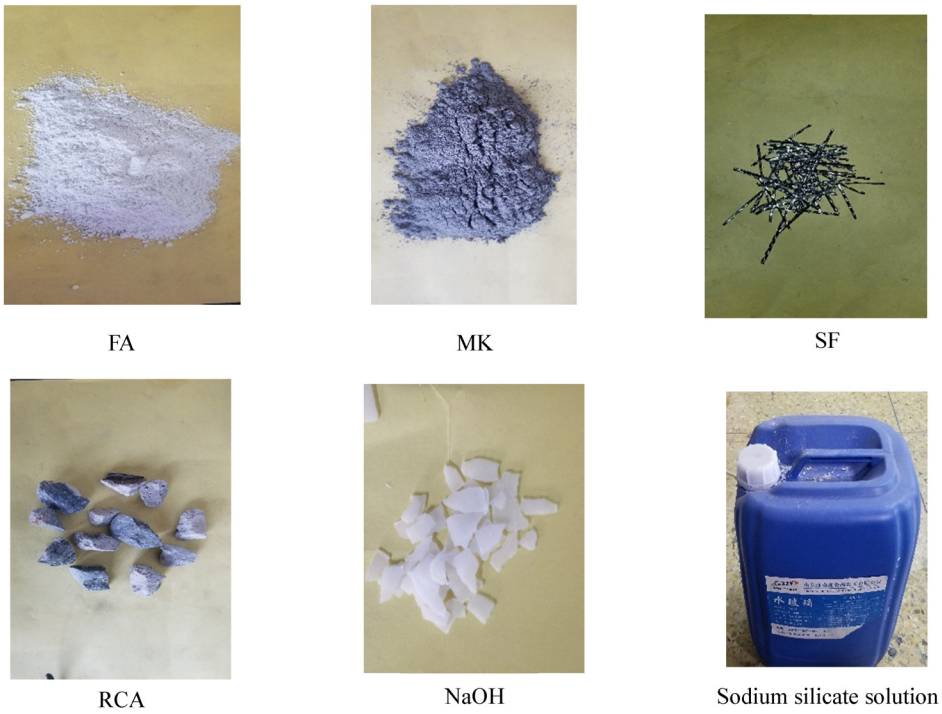

Figure 1: Photographs of materials.

Table 1: Chemical composition table of FA and MK

Materials	SiO_2	Al_2O_3	CaO	Fe_2O_3	TiO_2	SO_3	MgO	K_2O	Na_2O	Ignition loss
FA	50.80	28.10	3.70	6.20	0.00	1.80	1.20	0.60	1.20	7.90
MK	55.06	44.12	0.17	0.76	0.24	0.00	0.06	0.55	0.06	0.62

Table 2: Performance indicators of recycled coarse aggregate

Particle size (mm)	Water absorption (%)	Crushing index (%)	Apparent density (kg·m^{-3})
5–19	4.97	14.78	2,490

Table 3: Orthogonal test table

Level	Factors		
	Sand ratio	Aggregate cement material ratio	Modulus
1	0.40	3.00	1.20
2	0.35	3.50	1.10
3	0.30	4.00	1.00

of flake NaOH was greater than 99%. RCA was selected from the laboratory waste concrete block. SF with a tensile strength of 577 MPa and a density of 7,650 kg·m^{-3} was supplied by Changzhou Bochao Engineering Material Co. Ltd. The materials are shown in Figure 1, the fly ash (FA) and metakaolin (MK) are shown in Table 1, and the properties of coarse aggregates are shown in Table 2.

2.2 Orthogonal test and mix proportion design

The orthogonal test is a scientific method that can deal with multifactor and multilevel tests. Under the premise of ensuring accuracy, it can greatly reduce the number of tests [28,29]. For GPC and RAC, the modulus of alkali activator [30], the aggregate cementitious material ratio [31], and the sand ratio [32,33] have significant effects on their strength. Therefore, in this experiment, we use these three factors as variables and select three levels for each factor. With 7 days compressive strength as an indicator,

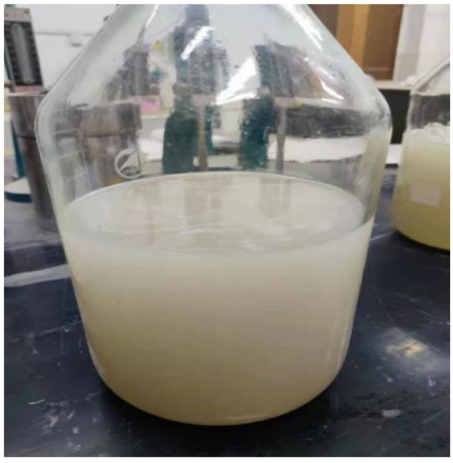

Figure 2: Alkali activator solution.

the ratio of the fixed water cementitious material is 0.30 and the ratio of FA/MK is 1:1 [34], The orthogonal test is carried out, and L9 (3^3) table is selected to arrange the test. At the same time, in order to avoid accidental errors, a range analysis was carried out on the test results. The orthogonal table is shown in Table 3, and the mix proportion is shown in Table 4.

2.3 Specimen preparation and curing

The alkali activator solution (NaOH, mixed sodium silicate solution) was prepared in advance and was left to cool to room temperature for 12 h, as shown in Figure 2.

Table 4: Design table of GRAC mix proportion (kg·m^{-3})

Test group	MK	FA	Sodium silicate	NaOH	Sand	Recycled aggregate	Sand ratio	Aggregate cement material ratio	Modulus
P1	295.33	295.33	301.32	36.15	708.79	1063.18	0.40	3.00	1.20
P2	265.49	265.49	270.80	39.81	743.36	1115.04	0.40	3.50	1.10
P3	241.07	241.07	245.89	43.28	771.43	1157.14	0.40	4.00	1.00
P4	294.44	294.44	300.33	44.15	618.32	1148.31	0.35	3.00	1.10
P5	264.71	264.71	270.00	47.52	648.53	1204.41	0.35	3.50	1.00
P6	242.32	242.32	247.16	29.66	678.49	1260.05	0.35	4.00	1.20
P7	293.48	293.48	299.35	52.69	528.26	1232.61	0.30	3.00	1.00
P8	266.21	266.21	271.53	32.58	559.04	1304.43	0.30	3.50	1.20
P9	241.72	241.72	246.53	36.24	580.13	1353.63	0.30	4.00	1.10

Note: The ratio of aggregate cementitious material is mass of (RCA + sand)/mass of (MK + FA); the ratio of water cementitious material is mass of sodium silicate solution solvent/mass of (MK + FA); sand ratio is the mass of sand/quality of (sand + RCA).

FA and MK were mixed for 60 s; soon after, the alkali activator solution was added and the mixture was stirred for 90 s. Then, SF was added to the mixture and it was stirred at a constant speed until the fibers were evenly distributed without coagulation and agglomeration, as shown in Figure 3. Finally, the aggregate was added and it was stirred for 120 s. After the mixture was stirred with all materials, it was poured into the mold and shook; soon after, it was placed with the film in an oven at 80°C and dried for 20 h [35,36] to demold, as shown in Figure 4. Later, it was dried in the open air (25°C) and was cured to the specified age [37,38], as shown in Figure 5. The whole production process is shown in Figure 6.

Figure 3: The process of casting concrete samples: (a) mixing concrete and (b) filling in the mold.

Figure 4: Maintenance of the cover film.

Figure 5: Concrete curing.

2.4 Test methods

2.4.1 Slump test

After the concrete was mixed, the slump cylinder was used to test the slump of different test groups within 5 min. The concrete needs to be filled three times. After each filling, a vibrating rod must be used to strike the barrel wall 25 times from the inside to the outside. After three fillings, the concrete on the surface of the slump is smoothed and then the slump is quickly lifted to measure its slump. The test process is shown in Figure 7.

2.4.2 Compressive strength test

Figure 8 shows the compressive strength test apparatus with the measuring accuracy of ±1%. Based on the previous experience and research results [39], the loading speed is set at 0.5 MPa·s^{-1}, and the average compressive strength of each test group is taken from three specimens. As the concrete specimens in this test are 100 mm × 100 mm × 100 mm nonstandard specimens, the compressive strength is calculated according to the following formula:

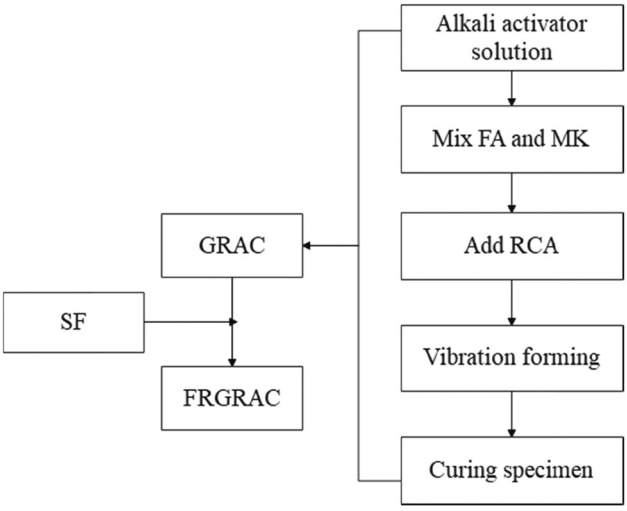

Figure 6: Production flow chart.

Figure 7: Slump test.

Figure 8: Compressive strength test apparatus.

$$f_{cu} = 0.95 \times \frac{F}{A} \tag{1}$$

where F is the compressive failure load and A is the bearing area of the specimen.

Figure 9: Tensile strength test apparatus.

2.4.3 Splitting tensile strength test

Figure 9 shows the tensile strength test apparatus. Wood chips are placed on the bottom of the fixture to ensure the stability of the specimen during testing. The specimen is put into the fixture and another piece of wood is placed on the top surface of the specimen to ensure stability and uniform force. The loading speed is set at 0.5 MPa·s^{-1}. As the concrete specimens in this test are 100 mm × 100 mm × 100 mm nonstandard specimens, the compressive strength is calculated according to the following formula:

$$f_{ts} = 0.85 \times \frac{2F}{\pi A} = 0.85 \times 0.637 \times \frac{F}{A} \tag{2}$$

where F is the splitting failure load (N) and A is the bearing area of the splitting (mm^2).

2.4.4 Flexural strength test

Figure 10 shows the flexural strength test apparatus. The positions of the two supports are adjusted according to the length of the test piece. The final distance between the two supports is 300 mm, and the distance between the two supports and the two sides of the concrete is approximately the same. The loading speed is set at 0.08 MPa·s^{-1}. As the concrete specimens in this test are 100 mm × 100 mm × 400 mm nonstandard specimens, the compressive strength is calculated according to the following formula:

$$f_f = 0.85 \times \frac{F_l}{bh^2} \tag{3}$$

where F is the flexural failure load (N), l is the support span (mm), b is the width of the specimen (mm). and h is the height of the test piece (mm).

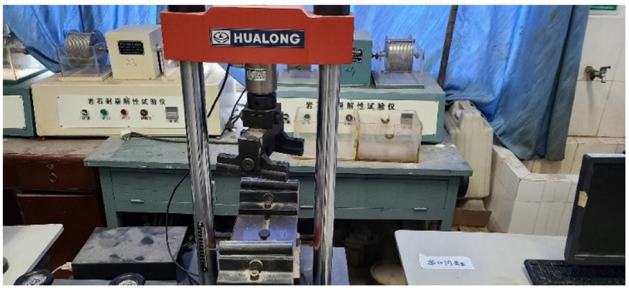

Figure 10: Flexural strength test apparatus.

2.5 SEM analysis

A scanning electron microscope is a type of electron microscope that generates sample images by scanning the surface with a focused electron beam, which is used to observe and test the surface microscopic morphology of the sample. The instrument used in this experiment is Prisma-E SEM equipment, as shown in Figure 11. The magnification of Prisma-E scanning electron microscope is 5–300,000 times, the subelectron resolution is 30 nm, the acceleration voltage is 0.3–30 kV (adjustable fixed bias), and the moving range of the sample is 100 mm inward, towards inner 50 mm, and 5.35 mm inward. The rotation angle is 360° and the temperature range is 20 + 90°.

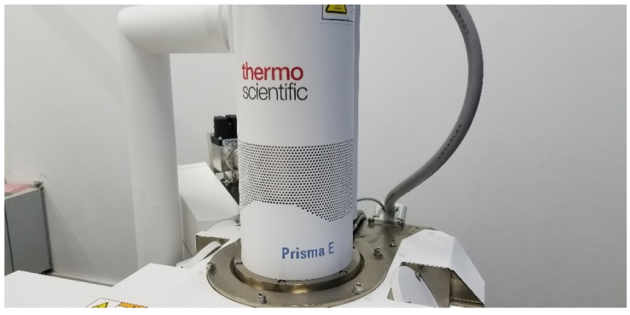

Figure 11: SEM observation apparatus.

3 Results and discussion

3.1 Orthogonal test results

The orthogonal test results are shown in Table 5, and the histogram is shown in Figure 12. It can be found from the figure that the 7 days compressive strength of the P5 group is the highest at 34.4 MPa, and the P1 group is the lowest at 18.2 MPa. The range analysis was performed on these results and the average value $\bar{k}$ and range value R of each factor level were calculated and are shown in Table 6. It can be found that the order of factors affecting the compressive strength of 7 days GRAC is sand ratio < aggregate cementitious material ratio < modulus. The average $\bar{k}$ of each factor level was used to make a trend chart, as shown in Figure 13. It can be seen from Figure 13 that both the sand ratio and the aggregate cementitious material ratio reach the maximum effect at 2 levels, and the effect on the 7 days compressive strength shows a trend of first increasing and then decreasing; however,

Table 5: Orthogonal test results

Test group	Sand ratio	Aggregate cement material ratio	Modulus	7 days compressive strength (MPa)
P1	0.40	3.00	1.20	18.2
P2	0.40	3.50	1.10	24.1
P3	0.40	4.00	1.00	26.8
P4	0.35	3.00	1.10	20.3
P5	0.35	3.50	1.00	34.4
P6	0.35	4.00	1.20	20.9
P7	0.30	3.00	1.00	27.8
P8	0.30	3.50	1.20	16.4
P9	0.30	4.00	1.10	24.4

the effect of the modulus increases and far exceeds the influence of the sand ratio and aggregate cementitious material ratio at 3 levels. The reason is that the alkali activator with a lower modulus has a higher alkali concentration (a higher OH^- concentration), which can promote the rupture of the Si–O and Al–O bonds in the geopolymer, and the strength is therefore continuously increased. On the other hand, there are $[SiO_4]$ groups in the sodium silicate solution. As the modulus decreases, the content of low-polymerization groups increases, which

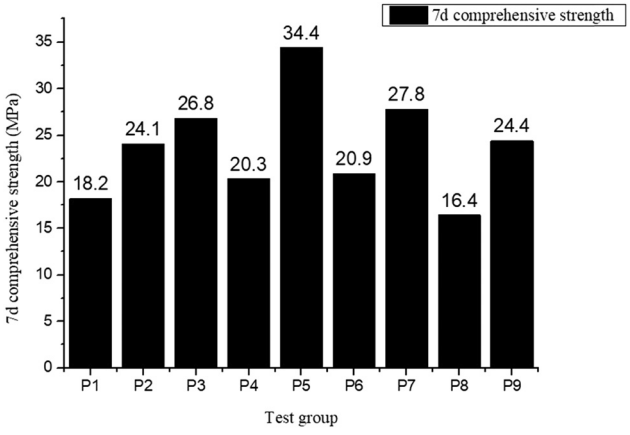

Figure 12: Orthogonal test results.

Table 6: Range analysis table

Factors	7 days compressive strength (MPa)			
		$\bar{k}$		R
Sand ratio	23.03	25.20	22.87	2.33
Aggregate cement material ratio	22.10	24.97	24.03	2.87
Modulus	18.50	22.93	29.67	11.17

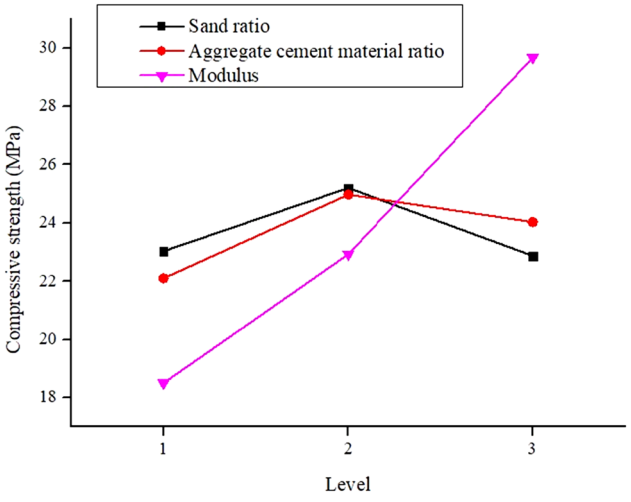

Figure 13: Trend chart of each factor level.

can also promote the rupture of the Si–O and Al–O bonds. In summary, based on the range analysis, the sand ratio is selected at 2 levels, the aggregate cementitious material ratio is selected at 2 levels, and the modulus is selected at 3 levels, which is the P5 test group. Based on the P5 test group, the effect of FRGRAC was studied by adding SF.

3.2 FRGRAC research results

On the basis of the P5 test group, SF was added to analyze the slump, compressive strength, tensile strength, and flexural strength of FRGRAC when the fiber content was 0.00, 0.50, 1.00, 1.50, 2.00, and 2.50%, respectively, The mix proportion of FRGRAC is shown in Table 7.

3.2.1 FRGRAC slump

No bleeding phenomenon was observed throughout the experiment. The FRGRAC slump results are shown in Figure 14. It can be observed from the figure that the slump of FRGRAC decreases continuously with the increase of fiber content. As the fiber content increases, the friction in the material continues to increase, which inhibits the flow of the material, and the fiber itself can also act as a bridge to prevent the material from slipping. On further observation, it was found that the slump difference between the M standard group and the SF-0.50 test group is the largest (31 mm), which is greater than the slump difference of the different fiber content test groups.

3.2.2 Compressive strength of FRGRAC

Figure 15 shows the FRGRAC 7 and 28 days compressive strength test results of each test group. It can be found that the 7 days compressive strength is 84.52% of the 28 days compressive strength of the M test group. At the same time, except for the 28 days SF-2.00 test group, the compressive strengths of the other groups increase with the increase of fiber content. When the fiber content was 2.50%, the compressive strength at 7 and 28 days were 38.97 and 47.1 MPa, respectively, which were 13.25 and 15.72% higher than that of the M group. The main reason for the above phenomenon is that the fiber can play a bridging role, helping to transfer and bear the stress, thereby increasing the compressive strength. At the same time, the fiber can also play the role of a hoop inside the concrete and can also improve the compressive strength under three-direction stress. But, on the other hand, due to the low crushing index of FRGRAC's recycled aggregate in this experiment, it has certain instability and the pouring process is not completed at one time. Therefore, some test groups may have higher aggregate residual mortar content, resulting in a decrease in the overall strength, such as the 28 days SF-2.00 test group. However, on the whole, the effect of fiber on the compressive strength of FRGRAC is more obvious and the optimal fiber content has not been found. In this respect, it is significantly different from GPC and RAC. Under

Table 7: FRGRAC mix proportion ($kg \cdot m^{-3}$)

Test group	MK	FA	Sodium silicate	NaOH	Sand	Recycled aggregate	SF
M	264.71	264.71	270.00	47.52	648.53	1204.41	0.00
SF-0.50	264.71	264.71	270.00	47.52	648.53	1204.41	38.25
SF-1.00	264.71	264.71	270.00	47.52	648.53	1204.41	76.50
SF-1.50	264.71	264.71	270.00	47.52	648.53	1204.41	114.75
SF-2.00	264.71	264.71	270.00	47.52	648.53	1204.41	153.00
SF-2.50	264.71	264.71	270.00	47.52	648.53	1204.41	191.25

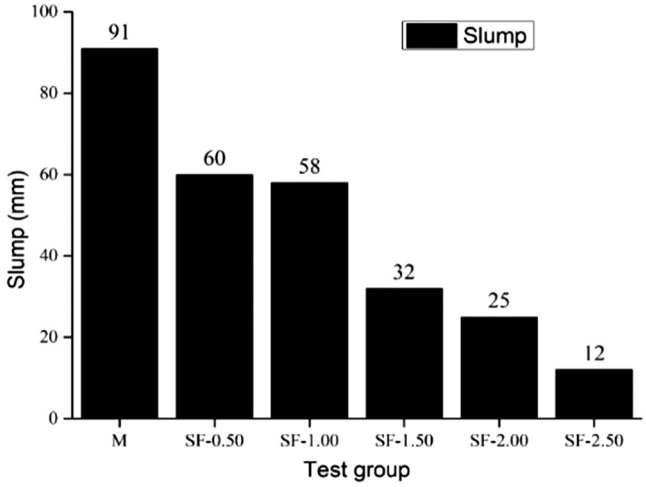

Figure 14: Slump test result.

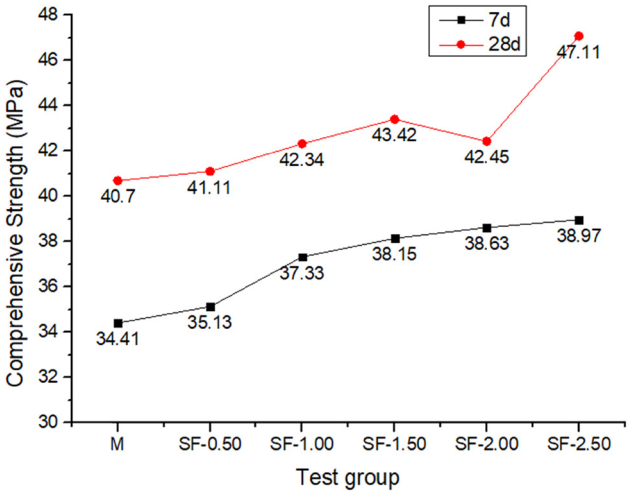

Figure 15: Compressive strength test results.

normal circumstances, the optimal content of fiber-reinforced GPC and RAC is between 1.0 and 1.5% [17–19]. This is due to the high ratio of water cementitious material. It can produce a large number of C–S–H gels. Even if the fiber content is increased, the C–S–H gel can still wrap the fibers tightly and not increase the porosity rate like in other types of concrete, thereby reducing the strength. On the other hand, because the strength of RCA in this test is low, the strength of FRGRAC made of recycled aggregate is affected by RCA, which does not show the strength of cementitious material itself. Therefore, even if a large amount of SF is added, it still does not reach the upper limit of the material strength and so the optimal content is not found.

Figure 16 shows the uniaxial compression test of the test block. It can be found that the damage of FRGRAC after the fiber addition is a failure with a certain amount of plastic deformation, indicating that the fiber strengthens the integrity of the test block and inhibits the generation of cracks.

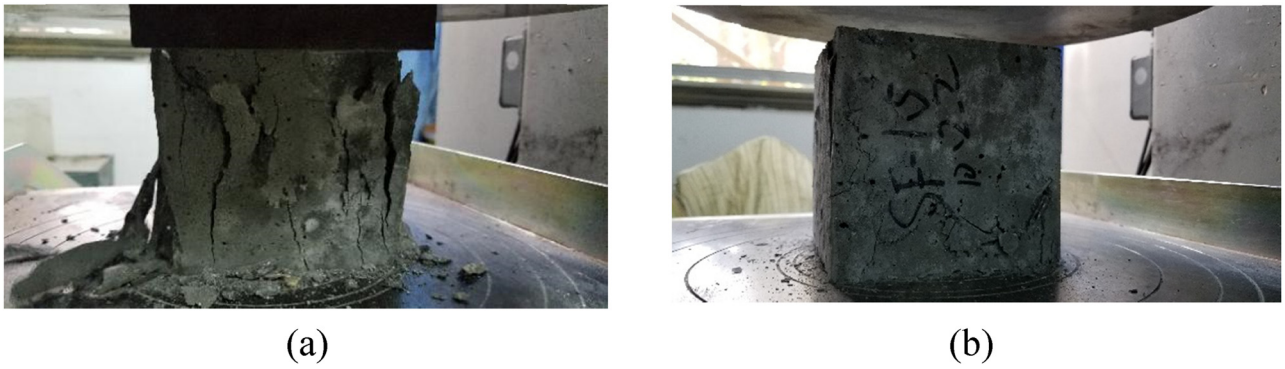

Figure 16: Test conditions of test block: (a) no added fiber specimen and (b) fiber-reinforced specimen.

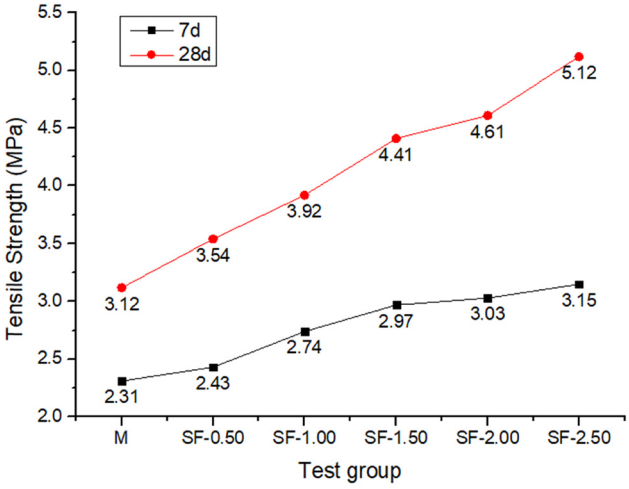

Figure 17: Tensile strength test results.

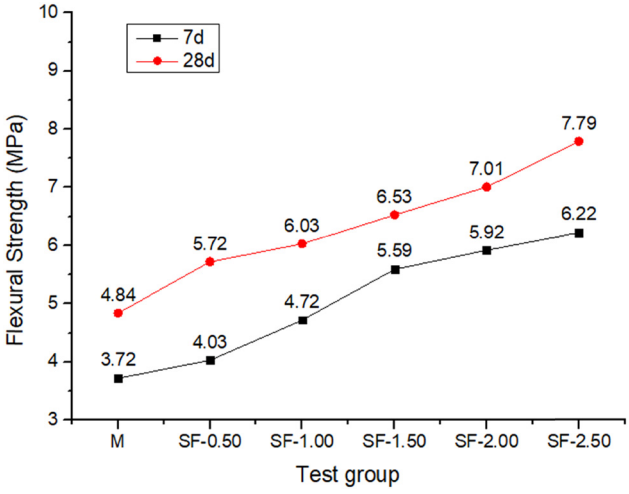

Figure 18: Flexural strength test results.

3.2.3 Tensile and flexural strength results of FRGRAC

Figures 17 and 18, respectively, show the tensile strength and flexural strength results of FRGRAC. It can be seen from Figure 17 that the tensile strength of FRGRAC increases continuously with the increase of fiber content and there is no inflection point. It shows that the incorporation of the fiber has a relatively continuous and stable improvement effect on the tensile strength of FRGRAC. When the fiber content is 2.5%, the tensile strengths of 7 and 28 days are 3.15 and 5.12 MPa, respectively, which are 36.36 and 64.10% higher than that of the *M* test group. This aspect is due to the high tensile strength of SF itself, which forms a stable three-dimensional grid system in the concrete, which improves the distribution, transmission, and bearing of stress, thereby enhancing the tensile strength.

On the other hand, it is also because of the good bonding performance between the SF and mortar. When the concrete cracks under tension, the fibers bear the main tensile stress. At this time, the fiber and the mortar are required to have good bonding properties. Further study can find that the improvement of the tensile strength of different test groups has a significant decrease in the 28 days SF-2.00 group, which is similar to the mechanism of the decrease of compressive strength. It also shows that the improvement of the tensile strength of FRGRAC by SF is better than that of compressive strength.

It can be found from Figure 18 that the flexural strength is the same as the tensile strength and both are steadily improved. When the fiber content is 2.5%, the flexural strength of 7 days and 28 days is 6.22 and 7.79 MPa, respectively, which are 67.2 and 60.95% higher than that of the *M* test group, and the degree of shaping is improved. The damage of the test block is shown in

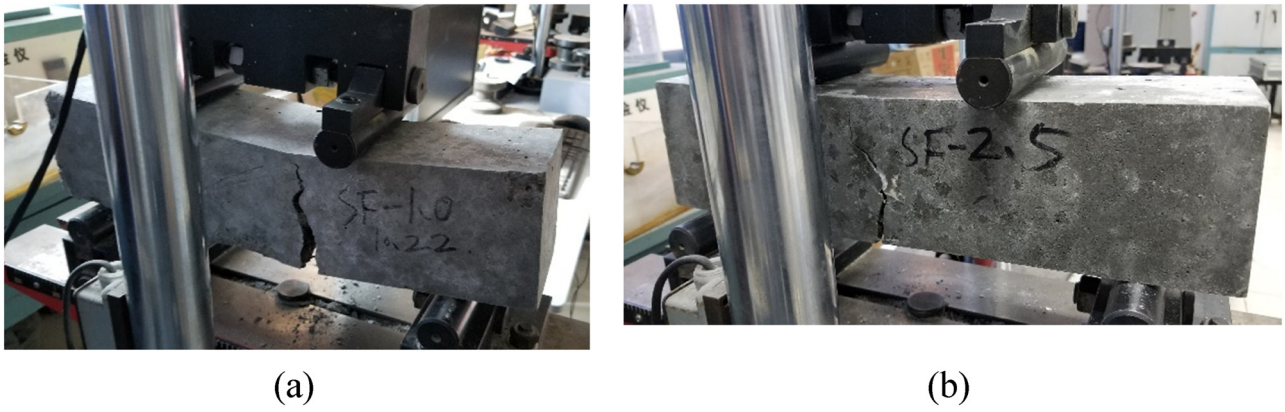

Figure 19: Flexural failure of test blocks with different fiber contents: (a) 1.00% fiber-reinforced specimen and (b) 2.50% fiber-reinforced specimen.

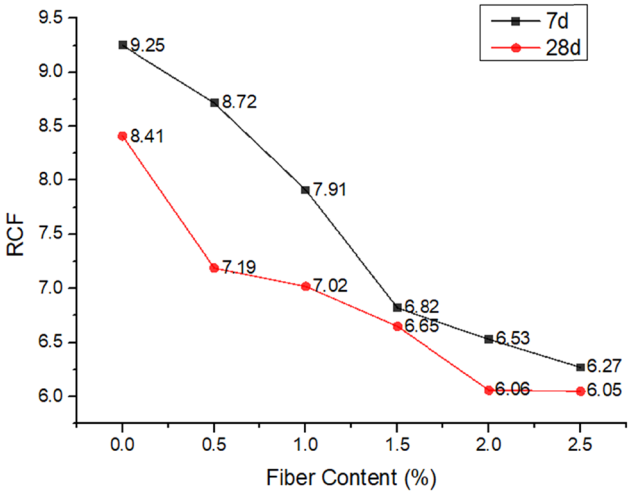

Figure 20: Effect of different fiber contents on RCF.

Figure 19. The modification mechanism is similar to the tensile strength and therefore it is not explained here.

Figure 20 shows the ratio of compressive strength/flexural strength (RCF) at 7 and 28 days. It can be found from the figure that the 7 days RCF of each test group is greater than the 28 days RCF. It shows that the plasticity of 7 days block is lower than that of 28 days block. With the increase of fiber content, the RCF of 7 or 28 days test block decreases, which indicates that fiber can improve the toughness of concrete at all ages.

3.2.4 SEM analysis of FRGRAC

In order to facilitate the comparative analysis, test groups M, SF-2.00, and SF-2.50 of 28 days are selected, as shown

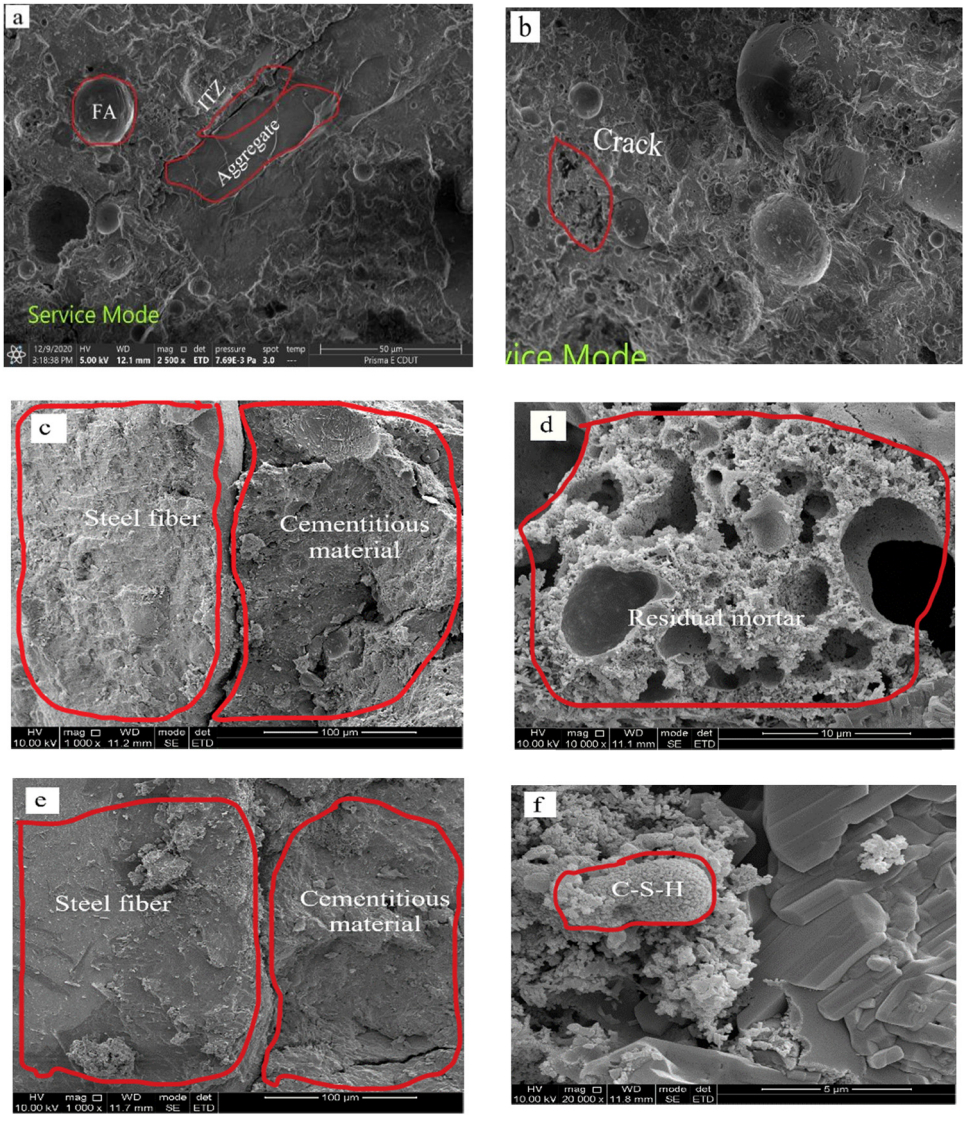

Figure 21: SEM analysis results: (a) M test group interface; (b) micro cracks; (c) bonding between steel fiber and cementitious material in SF-2.0 test group; (d) residual mortar; (e) bonding between steel fiber and cementitious material in SF-2.5 test group; (f) distribution of C–S–H gel.

in Figure 21. Figure 21a and b shows the situation of the M test group, and more unreacted FA particles can be found. This is mainly due to the insufficient polymerization reaction at room temperature during the curing process and many cracks and holes can also be found. Figure 21c and d shows the situation of the SF-2.00 test group. In the figure, it is found that SF is embedded in the matrix and can bear the stress together and play the role of a bridge. However, it is also found that there are gaps between the bonding surface and the cementitious material. At the same time, it can be seen that the residual mortar has a large number of holes and the texture is fluffy. If the content of the residual mortar is high, it will undoubtedly reduce the strength of FRGRAC. Figure 21e and f shows the SF-2.50 test group. It can be found that SF has a tighter bond with the cementitious material. The C–S–H gel is also tightly bound to the aggregate. The polymerization reaction is more complete than the other test groups. This is an intuitive reason for the higher intensity of the test group.

4 Conclusion

This study has explored the optimum mix proportion of FA–MK geopolymer recycled concrete through orthogonal design. Building on this, the mechanical properties of fiber-reinforced geopolymer-recycled concrete with different SF contents were investigated. Followed by this, the specimens were analyzed by SEM. The main conclusions are as follows.

(1) The mechanical properties of FRGRAC were studied by using SF with FA–MK-based GRAC. The results from the orthogonal test indicate that the order of the factors affecting the 7 days compressive strength of FA–MK-based GRAC is sand ratio < aggregate cementitious material ratio < modulus. When the ratio of water cementitious material is 0.30, the sand ratio is 0.35, and the aggregate cementitious material ratio is 3.50; the 7 days compressive strength of GRAC block with a modulus of 1.00 can reach 34.4 MPa.
(2) As the content of SF increases, the slump continues to decrease and the compressive strength, tensile strength, and flexural strength of FRGRAC have all been improved to a certain extent, and no optimum dosage has been found. When the fiber content is 2.50%, the 7 days compressive strength, tensile strength, and flexural strength are increased by 13.25, 36.36, and 67.2%, respectively, compared with the M group. Compared with the performance of 7 days FRGRAC, SF improves the performance of 28 days FRGRAC more significantly. When the fiber content is 2.50%, the 28 days compressive strength, tensile strength, and flexural strength are increased by 15.72, 64.10, and 60.95%, respectively, compared with those of the M group.
(3) It was found by SEM that the fibers resisted the formation of cracks. Some test groups contained more unreacted FA particles, which were mainly due to the limitation of the curing temperature. The residual mortar has a higher porosity. When the residual mortar content of the test group increased, the strength decreased significantly.

Acknowledgements: This study was supported by the Open Project of Chongqing groundwater Resources Utilization and Environmental Protection Laboratory (DXS20191029), Sichuan Science and Technology Program (2020JDR0266, 2019YFG0460), Chongqing Innovation and Application Development Special General Project (cstc2020jscx-msxmX0084), Sichuan Mingyang Construction Engineering Management Co. Ltd. Special Research Project (MY2021-001).

Funding information: This study was supported by the Open Project of Chongqing groundwater Resources Utilization and Environmental Protection Laboratory (DXS20191029), Sichuan Science and Technology Program (2020JDR0266, 2019YFG0460), Chongqing Innovation and Application Development Special General Project (cstc2020jscx-msxmX0084), and Sichuan Mingyang Construction Engineering Management Co., Ltd. Specialized project (MY2021-001).

Author contributions: Zhong Xu, Zhenpu Huang, and Changjiang Liu wrote the article. Xiaowei Deng, David Hui, Yuting Deng, Min Zhao, and Libing Qin checked the manuscript.

Conflict of interest: One of the co-authors - Prof. David Hui - is an Editor in Chief of Reviews on Advanced Materials Science.

Data availability statement: All data generated or analyzed during this study are included in this published article or are available from the corresponding author on reasonable request.

References

[1] Navid, R. and M. Z. Zhang. Fiber-reinforced geopolymer composites: A review. *Cement and Concrete Composites*, Vol. 107, 2020, id. 103498.

[2] Sun, Y. F., Y. Y. Peng, T. S. Zhou, H. W. Liu, and P. W. Gao. Study of the mechanical-electrical-magnetic properties and the microstructure of three-layered cement-based absorbing boards. *Reviews on Advanced Materials Science*, Vol. 59, No. 1, 2020, pp. 160–169.
[3] Liu, C. J., X. C. Huang, Y. Y. Wu, X. W. Deng, and Z. L. Zheng. The effect of graphene oxide on the mechanical properties, impermeability and corrosion resistance of cement mortar containing mineral admixtures. *Construction and Building Materials*, Vol. 288, 2021, id. 123059.
[4] Reiterman, P., O. Holčapek, O. Zobal, and M. Keppert. Freeze-thaw resistance of cement screed with various supplementary cementitious materials. *Reviews on Advanced Materials Science*, Vol. 58, No. 1, 2019, pp. 66–74.
[5] Silva, D. P., K. S. Crenstil, and V. Sirivivatnanon. Kinetics of geopolymerization: Role of Al_2O_3 and SiO_2. *Cement and Concrete Composites*, Vol. 37, No. 4, 2007, pp. 512–518.
[6] He, J., Y. X. Jie, J. H. Zhang, and G. P. Zhang. Synthesis and characterization of red mud and rice husk ash-based geopolymer composites. *Cement and Concrete Composites*, Vol. 37, 2013, pp. 108–118.
[7] Sevinc, A. H. and M. Y. Durgun. Properties of high-calcium fly ash-based geopolymer concretes improved with high-silica sources. *Construction and Building Materials*, Vol. 261, 2020, id. 120014.
[8] Liu, C. J., X. W. Deng, J. Liu, and D. Hui. Mechanical properties and microstructures of hypergolic and calcined coal gangue based geopolymer recycled concrete. *Construction and Building Materials*, Vol. 221, 2019, pp. 691–708.
[9] Koushkbaghi, M., P. Alipour, B. Tahmouresi, E. Mohseni, A. Saradar, and P. K. Sarker. Influence of different monomer ratios and recycled concrete aggregate on mechanical properties and durability of geopolymer concretes. *Construction and Building Materials*, Vol. 205, 2019, pp. 519–528.
[10] Zhu, P. H., M. Q. Hua, H. Liu, X. J. Wang, and C. H. Chen. Interfacial evaluation of geopolymer mortar prepared with recycled geopolymer fine aggregates. *Construction and Building Materials*, Vol. 259, 2020, id. 119849.
[11] Xu, Z., Z. P. Huang, C. J. Liu, X. W. Deng, and D. Hui. Research progress on mechanical properties of geopolymer recycled aggregate concrete. *Reviews on Advanced Materials Science*, Vol. 60, 2021, pp. 158–172.
[12] Tang, Z., W. G. Li, V. W. Y. Tam, and L. B. Yan. Mechanical performance of CFRP-confined sustainable geopolymeric recycled concrete under axial compression. *Engineering Structures*, Vol. 224, 2020, id. 111246.
[13] Khan, M. Z. N., Y. F. Hao, H. Hao, and F. U. A. Shaikh. Mechanical properties of ambient cured high strength hybrid steel and synthetic fibers reinforced geopolymer composites. *Cement and Concrete Composites*, Vol. 85, 2018, pp. 133–152.
[14] Liu, C. J., X. C. Huang, Y. Y. Wu, X. W. Deng, J. Liu, Z. L. Zheng, et al. Review on the research progress of cement-based and geopolymer materials modified by graphene and graphene oxide. *Nanotechnology Reviews*, Vol. 9, No. 1, 2020, pp. 155–169.
[15] Liu, C. J., X. C. Huang, Y. Y. Wu, X. W. Deng, Z. L. Zheng, Z. Xu, et al. Advance on the dispersion treatment of graphene oxide and the graphene oxide modified cement-based materials. *Nanotechnology Reviews*, Vol. 10, No. 1, 2021, pp. 34–49.
[16] Saloni, P. and T. M. Pham. Enhanced properties of high-silica rice husk ash-based geopolymer paste by incorporating basalt fibers. *Construction and Building Materials*, Vol. 245, 2020, id. 118422.
[17] Faris, M. A., M. M. Abdullah, R. Muniandy, M. F. Abu Hashim, K. Błoch, B. Jeż, et al. Comparison of hook and straight steel fibers addition on malaysian fly ash-based geopolymer concrete on the slump, density, water absorption and mechanical properties. *Materials*, Vol. 14, No. 5, 2021, id. 1310.
[18] Yang, M. J., P. S. Raj, and Z. J. Gao. Snow-proof roadways using steel fiber-reinforced fly ash geopolymer mortar-concrete. *Journal of Materials in Civil Engineering*, Vol. 33, No. 2, 2021, id. 04020444.
[19] El-Sayed, T. A. and Y. B. I. Shaheen. Flexural performance of recycled wheat straw ash-based geopolymer Rc beams and containing recycled steel fiber. *Structures*, Vol. 28, 2020, pp. 1713–1728.
[20] Qureshi, L. A., B. Ali, and A. Ali. Combined effects of supplementary cementitious materials (silica fume, GGBS, fly ash and rice husk ash) and steel fiber on the hardened properties of recycled aggregate concrete. *Construction and Building Materials*, Vol. 263, 2020, id. 120636.
[21] Zong, S., Z. Liu, S. Li, Y. Lu, and A. Zheng. Stress-strain behavior of steel-fiber-reinforced recycled aggregate concrete under axial tension. *Journal of Cleaner Production*, Vol. 278, 2021, id. 123248.
[22] Huang, Y. J., J. Z. Xiao, L. Qin, and P. Li. Mechanical behaviors of GFRP tube confined recycled aggregate concrete with sea sand. *Advances in Structural Engineering*, Vol. 24, No. 6, 2021, pp. 1196–1207.
[23] Liu, C. J., X. He, X. W. Deng, Y. Y. Wu, Z. L. Zheng, J. Liu, et al. Application of nanomaterials in ultra-high performance concrete: a review. *Nanotechnology Reviews*, Vol. 9, No. 12, 2020, pp. 1427–1444.
[24] Etxeberria, M., E. Vazquez, A. Mari, and M. Barra. Influence of amount of recycled coarse aggregates and production process on properties of recycled aggregate concrete. *Cement and Concrete Research*, Vol. 37, No. 5, 2007, pp. 735–742.
[25] Rao, A., K. Jha, and S. Misra. Use of aggregates from recycled construction and demolition waste in concrete. *Resources Conservation and Recycling*, Vol. 50, No. 1, 2007, pp. 71–81.
[26] Lu, W. and H. Yuan. A framework for understanding waste management studies in construction. *Waste Management*, Vol. 31, No. 6, 2011, pp. 1252–1260.
[27] Le, H. B., Q. B. Bui, and L. P. Tang. Geopolymer recycled aggregate concrete: from experiments to empirical models. *Materials*, Vol. 14, No. 5, 2021, id. 1180.
[28] Liang, C., Y. Q. Liu, and Y. Q. Liu. An orthogonal component method for steel girder-concrete abutment connections in integral abutment bridges. *Journal of Constructional Steel Research*, Vol. 180, 2021, id. 106604.
[29] Tang, Z. *Experimental study on engineering characteristics of geopolymer recycled concrete road base*, Southeast University, Nanjing, 2017 (in Chinese).
[30] Chamila, G., A. Peter, L. Weena, L. David, and S. Sujeeva. Novel analytical method for mix design and performance prediction of high calcium fly ash geopolymer concrete. *Polymers*, Vol. 13, No. 6, 2021, id. 900.
[31] Xie, H. L., H. Fang, W. Cai, L. Wan, and R. L. Huo. Development of an innovative composite sandwich matting with GFRP facesheets and wood core. *Reviews on Advanced Materials Science*, Vol. 60, No. 1, 2021, pp. 80–91.

[32] Katinas, E., R. Choteborsky, M. Linda, and J. Kure. Sensitivity analysis of the influence of particle dynamic friction, rolling resistance and volume/shear work ratio on wear loss and friction force using DEM model of dry sand rubber wheel test. *Tribology International*, Vol. 156, 2021, id. 106853.
[33] Lian, S. S., T. Meng, H. Q. Song, Z. J. Wang, and J. B. Li. Relationship between percolation mechanism and pore characteristics of recycled permeable bricks based on X-ray computed tomography. *Reviews on Advanced Materials Science*, Vol. 60, No. 1, 2021, pp. 207–215.
[34] Zhang, H. Y., S. L. Qi, and L. Cao. Thermal behavior and mechanical properties of geopolymer mortar after exposure to elevated temperatures. *Construction and Building Materials*, Vol. 109, 2015, pp. 17–24.
[35] Wang, J. J., J. H. Xie, C. H. Wang, J. B. Zhao, F. Liu, and C. Fang. Study on the optimum initial curing condition for fly ash and GGBS based geopolymer recycled aggregate concrete. *Construction and Building Materials*, Vol. 247, 2020, id. 118540.
[36] Jahangir, A., F. Malik, N. Muhammad, and R. Fayyaz. Reflection phenomena of waves through rotating elastic medium with micro-temperature effect. *Reviews on Advanced Materials Science*, Vol. 59, No. 1, 2020, pp. 455–463.
[37] Luan, C. C., Q. Y. Wang, and F. H. Yang. Practical prediction models of tensile strength and reinforcement-concrete bond strength of low-calcium fly ash geopolymer concrete. *Polymers*, Vol. 13, 2021, id. 875.
[38] Ahmad, S. I., H. Hamoudi, A. Abdala, and Z. K. Ghouri. Graphene-reinforced bulk metal matrix composites: synthesis, microstructure, and properties. *Reviews on Advanced Materials Science*, Vol. 59, No. 1, 2020, pp. 67–114.
[39] Ganesh, A. C. and M. Muthukannan. Development of high performance sustainable optimized fiber reinforced geopolymer concrete and prediction of compressive strength. *Journal of Cleaner Production*, Vol. 282, 2021, id. 124543.